Transport coefficients for granular media from molecular dynamics simulations

C. Bizon, M. D. Shattuck, J. B. Swift, and Harry L. Swinney

Center for Nonlinear Dynamics and Department of Physics, University of Texas, Austin, Texas 78712

Under many conditions, macroscopic grains flow like a fluid; kinetic theory predicts continuum equations of motion for this granular fluid. In order to test the theory, we perform event-driven molecular simulations of a two-dimensional gas of inelastic hard disks, driven by contact with a heat bath. Even for strong dissipation, high densities, and small numbers of particles, we find that continuum theory describes the system well. With a bath that heats the gas homogeneously, strong velocity correlations produce a slightly smaller energy loss due to inelastic collisions than that predicted by kinetic theory. With an inhomogeneous heat bath, thermal or velocity gradients are induced. Determination of the resulting fluxes allows calculation of the thermal conductivity and shear viscosity, which are compared to the predictions of granular kinetic theory, and which can be used in continuum modeling of granular flows. The shear viscosity is close to the prediction of kinetic theory, while the thermal conductivity can be overestimated by a factor of 2; in each case, transport is lowered with increasing inelasticity. [S1063-651X(99)03310-3]

PACS number(s): 45.70.−n, 66.90.+r, 05.20.Dd, 02.70.Ns

I. INTRODUCTION

Collections of inelastically colliding macroscopic particles, when driven sufficiently by an external force, exhibit fluidlike behavior such as flow [1,2] and instabilities similar to those seen in liquids [3,4]. Although only a small number of particles (10^2–10^6) are typically involved in a flow, continuum methods are popular tools in modeling, because a century of fluid dynamics experience can be brought to bear on the problem. With continuum equations velocity profiles and transfer rates can be calculated, and stability analyses performed. Often, plausible continuum equations are simply posited, but these equations typically contain unmeasurable free parameters. A more rigorous approach derives continuum equations from the kinetic theory of dissipative gases [5–7]. In principle, a closed system of partial differential equations results, analogous to the Navier-Stokes equations, with all transport coefficients given.

However, the continuum equations for granular media do not share the stature of their molecular fluid analogs. For both grains and molecules, the general form of the equations is not in question, but the constitutive equations relating fluxes of momentum and energy to gradients may differ from the simple cases of Newton's viscosity law and Fourier's heat law. The transport coefficients of liquids are not routinely calculated from kinetic theory, but are measured experimentally; such measurements have not been carried out for granular media, where the granular temperature (the kinetic energy associated with the fluctuational velocities of particles) is difficult to control and difficult to measure. In addition, the small number of particles, long mean free paths, and the dissipative nature of the medium have led some researchers to the conclusion that continuum approaches are doomed to failure [8,9].

As a result, the central question remains open: *Can continuum equations, derived from kinetic theory and supplemented by measurements, model rapid granular flows to the same level that Navier-Stokes equations model the flows of liquids?* Molecular dynamics simulations will play a crucial

role in answering this question, since the data they provide can be used to quantitatively test the assumptions and the results of kinetic theory.

The main assumptions [5–7], which we will elucidate in Sec. II, are (1) single-particle velocity distribution functions are nearly Boltzmann, (2) molecular chaos–particle velocities are uncorrelated, and (3) particle positions are correlated in accord with Eq. (5), the Carnahan and Starling relation for elastic particles.

The main results, also discussed further in Sec. II, are (1) the equation of state [Eq. (13)], (2) the constitutive relations [Newton's stress law and Fourier's heat law—Eqs. (11) and (12)], and (3) the values of the shear viscosity μ, the thermal conductivity κ, and the loss rate of granular temperature due to inelastic collisions, γ [Eqs. (16), (17), and (14)].

We will use molecular dynamics simulations to test these points, and to measure the transport coefficients to be used in continuum analyses of granular flows. We have found that the simulations quantitatively reproduce experiments on standing waves in oscillated granular media, producing the correct wave patterns and wavelengths [10] and secondary instabilities [4]. With the numerical simulation, we not only have access to experimentally unmeasurable quantities [11], but we also can study systems that are not experimentally realizable, allowing us to test both the assumptions and results of the granular kinetic theory. Once the constitutive relations have been tested and possibly enhanced through the use of particle simulations, direct comparison between continuum theory and laboratory experiment becomes possible. We compare directly to the results of Ref. [7], but many of the kinetic theories are similar in spirit. We do not, however, consider more sophisticated theories that include long-range spatial correlations [12] or recollision effects [13].

Laboratory tests of granular kinetic theory have not yet proceeded beyond measuring the single-particle velocity distribution function [14–16]. Simulations that make contact with kinetic theory have focused mainly on the homogeneous cooling state, a time-dependent state that eventually becomes spatially inhomogeneous. In those simulations, long-range velocity correlations develop [17], and molecular

chaos no longer holds. A more sophisticated form of kinetic theory, ring kinetic theory, in which correlations in particle velocity are accounted for, is required for a full description [18]. A simulation on a granular gas between two walls with different granular temperatures shows that in the quasielastic limit, granular kinetic theory produces good temperature profiles [19]. Finally, a number of simulations have been performed on granular media in contact with a heat bath [20–22] to produce a steady state. In one dimension (1D), spatial [20] and velocity [21] correlations can develop, and the single-particle velocity distributions may be non-Gaussian [22]. Recent results on a randomly driven two-dimensional system show long-range correlations in good agreement with a mode-coupling theory [12].

In Sec. III we describe the molecular dynamics simulations and the forcing methods. Section IV discusses simulations of granular media in which the heat bath is spatially homogeneous. In that section, we will check the assumptions about the nature of the single-particle distribution function and the correlations of position and velocity, as well as measuring the equation of state and γ. In Sec. V we turn to our main purpose: allowing the heat bath to vary spatially so that stationary inhomogeneous states may be induced and described. From these simulations we can study the constitutive relations, the shear viscosity, and the thermal conductivity. Section VI contains concluding remarks.

II. KINETIC THEORY

We begin with a brief review of the kinetic theory of granular media, which differs only slightly from the kinetic theory of elastic particles as presented in textbooks such as [23]. Specifically, we discuss kinetic theory as described by Jenkins and Richman [6,7], but most of the kinetic theories in the literature are similar [5,24–26]. The number of particles in a volume and velocity element $d\mathbf{r}d\mathbf{v}$ centered at position $\mathbf{r}$ and velocity $\mathbf{v}$ is given by $f^{(1)}(\mathbf{r},\mathbf{v},t)d\mathbf{r}d\mathbf{v}$; $f^{(1)}(\mathbf{r},\mathbf{v},t)$ is called the single-particle distribution function. Continuum quantities are given as averages over $f^{(1)}(\mathbf{r},\mathbf{v},t)$. In particular, the number density, average velocity, and granular temperature are defined, respectively, as

$$n(\mathbf{r},t) \equiv \int f^{(1)}(\mathbf{r},\mathbf{v},t)d\mathbf{v}, \qquad (1)$$

$$\mathbf{v}_0(\mathbf{r},t) \equiv \frac{1}{n}\int f^{(1)}(\mathbf{r},\mathbf{v},t)\mathbf{v}d\mathbf{v}, \qquad (2)$$

$$T(\mathbf{r},t) \equiv \frac{1}{nD}\int f^{(1)}(\mathbf{r},\mathbf{v},t)(\mathbf{v}-\mathbf{v}_0)^2 d\mathbf{v}, \qquad (3)$$

where D is the number of dimensions. Note that the granular temperature T is not the thermodynamic temperature of the particles due to the random motions of their molecules, but the analogous kinetic energy due to the random motions of the macroscopic particles themselves.

The evolution of $f^{(1)}(\mathbf{r},\mathbf{v},t)$ depends on the joint probability distribution, $f^{(2)}(\mathbf{r}_1,\mathbf{v}_1,\mathbf{r}_2,\mathbf{v}_2,t)$; collisions of two particles change the single-particle distribution. As in molecular kinetic theory, Boltzmann's assumption of molecular chaos is made, i.e., velocities are assumed to be uncorrelated, although for sufficiently dense media, positional correlations are allowed:

$$f^{(2)}(\mathbf{r}_1,\mathbf{v}_1,\mathbf{r}_2,\mathbf{v}_2,t) = g(\sigma,\nu)f^{(1)}(\mathbf{r}_2 \\ -\sigma\hat{\mathbf{k}},\mathbf{v}_1,t)f^{(1)}(\mathbf{r}_2,\mathbf{v}_2,t), \qquad (4)$$

where σ is the particle radius, $\hat{\mathbf{k}}$ is a unit vector pointing from the center of particle 1 to the center of particle 2, and $\nu = \frac{1}{4}n\pi\sigma^2$ is the solid fraction in 2D.

The positional correlations are accounted for through $g(r,\nu)$, the radial distribution function, which is defined as the probability of having a pair of particles whose relative distance lies in the interval $r,r+dr$, normalized by the probability for an ideal gas. This function, evaluated at the point of contact $r=\sigma$, gives the increase in the probability of collisions due to dense gas (excluded volume) corrections. For elastic hard disks, spatial correlations are described by the formula of Carnahan and Starling [27],

$$G_{CS}(\nu) = \frac{\nu(16-7\nu)}{16(1-\nu)^2}, \qquad (5)$$

where

$$G(\nu) \equiv \nu g(\sigma,\nu). \qquad (6)$$

Equation (5) works well for elastic particles with solid fractions below 0.675, where a phase transition takes place [28], and is often used in modeling granular media [7]. Equation (6) is the definition of G in terms of the (unknown) radial distribution function $g(r,\nu)$, evaluated at $r=\sigma$, while Eq. (5) is a particular model for G, denoted by the subscript CS.

An unforced collection of elastic particles approaches a Boltzmann distribution,

$$f^{(1)}(\mathbf{r},\mathbf{v},t) = n(2\pi T)^{-D/2}e^{-C^2/2T}, \qquad (7)$$

where $C \equiv |\mathbf{v}-\mathbf{v}_0|$. Away from equilibrium, the local distribution for elastic particles is nearly Boltzmann. Granular media dissipate energy with each collision, so that the equilibrium state of an unforced granular medium is that of no relative motion. For grains, the single-particle distribution function is simply assumed to be nearly a Boltzmann distribution.

With these assumptions, and the additional assumption that the coefficient of restitution e is only slightly less than 1 (particles are only slightly inelastic), equations for the continuum mass, momentum, and energy can be derived for disks in two dimensions [6,7]:

$$\frac{\partial n}{\partial t} + \boldsymbol{\nabla}\cdot(n\mathbf{v}_0) = 0, \qquad (8)$$

$$n\frac{\partial\mathbf{v}_0}{\partial t} + n\mathbf{v}_0\cdot\boldsymbol{\nabla}\mathbf{v}_0 = -\boldsymbol{\nabla}\cdot\underline{P}, \qquad (9)$$

$$n\frac{\partial T}{\partial t} + n\mathbf{v}_0\cdot\boldsymbol{\nabla}T = -\boldsymbol{\nabla}\cdot\mathbf{q} - \underline{P}{:}\underline{E} - \gamma, \qquad (10)$$

where $E_{ij} = \frac{1}{2}(\partial_i v_{0j} + \partial_j v_{0i})$ are the elements of the symmetrized velocity gradient tensor $\underline{\mathbf{E}}$. The constitutive relation for the pressure tensor $\underline{\mathbf{P}}$ is Newton's stress law,

$$\underline{\mathbf{P}} = (P - 2\lambda \, \mathrm{Tr} \, \underline{\mathbf{E}})\underline{\mathbf{I}} - 2\mu[\underline{\mathbf{E}} - (\mathrm{Tr} \, \underline{\mathbf{E}})\underline{\mathbf{I}}], \qquad (11)$$

where Tr denotes trace and $\underline{\mathbf{I}}$ is the unit tensor. For the heat flux $\mathbf{q}$, the constitutive relation is Fourier's heat law,

$$\mathbf{q} = -\kappa \boldsymbol{\nabla} T. \qquad (12)$$

The 2D equations close [7] with the equation of state, which is the ideal gas equation of state with a term that includes dense gas and inelastic effects,

$$P = (4/\pi\sigma^2)\nu T[1 + (1+e)G(\nu)], \qquad (13)$$

and the predicted values, denoted with a subscript 0, for the temperature loss rate per unit volume γ,

$$\gamma_0 = \frac{16\nu G(\nu)}{\sigma^3}(1-e^2)\left(\frac{T}{\pi}\right)^{3/2}, \qquad (14)$$

and the transport coefficients, which take on the Enskog values: the bulk viscosity λ,

$$\lambda_0 = \frac{8\nu G(\nu)}{\pi\sigma}\sqrt{\frac{T}{\pi}}, \qquad (15)$$

the shear viscosity μ,

$$\mu_0 = \frac{\nu}{2\sigma}\left[\frac{1}{G(\nu)} + 2 + \left(1 + \frac{8}{\pi}\right)G(\nu)\right]\sqrt{\frac{T}{\pi}}, \qquad (16)$$

and the thermal conductivity κ,

$$\kappa_0 = \frac{2\nu}{\sigma}\left[\frac{1}{G(\nu)} + 3 + \left(\frac{9}{4} + \frac{4}{\pi}\right)G(\nu)\right]\sqrt{\frac{T}{\pi}}. \qquad (17)$$

Because of the assumption of near elasticity, the coefficient of restitution enters only in the equation of state and in the expression for the temperature loss due to inelastic collisions. To this order, the thermal conductivity and viscosities predicted by inelastic kinetic theory are the same as those given by the Enskog procedure for elastic disks [29].

III. DRIVEN GRANULAR MEDIA SIMULATIONS

We perform event-driven simulations [30,31] of a granular gas in a two-dimensional periodic box of side length $L = 52.6\sigma$, in contact with a thermal bath that stochastically heats particles throughout the volume. Between collisions, particles travel freely. In our model the collisions are instantaneous and binary; they conserve momentum and dissipate energy. Particles are assumed to be frictionless; particle friction can be incorporated into kinetic theories [24,25], and was included in the simulations of oscillated granular media [10,11,4], but introduces complications that we wish to avoid for this study.

When particles collide, new velocities are calculated by reversing the component of the relative particle velocity along the line joining particle centers and multiplying it by the coefficient of restitution e, which is between 0 and 1. If e

is independent of collision velocity, a finite time singularity can occur in the collision frequency, a phenomenon known as inelastic collapse [32,33]. In real materials, however, the coefficient of restitution is a function of collision velocity [34,35]. To avoid the simulation-ending inelastic collapse, we allow e to vary [36] as

$$e(v_n) = \begin{cases} 1 - B v_n^\beta, & v_n < v_a \\ \epsilon, & v_n > v_a \end{cases} \qquad (18)$$

where v_n is the component of relative velocity along the line joining particle centers (normal to the contact surface), $B = (1-\epsilon)(v_a)^{-\beta}$, $\beta = 3/4$, and ϵ is a constant, chosen to be 0.7. In simulations of oscillated granular media, the results are not sensitively dependent on v_a or β, and $\epsilon = 0.7$ produces good agreement with experiment [4,10,11]. In addition to forestalling collapse, variation of e allows us to further probe granular kinetic theory, which assumes that $e \approx 1$. As T varies, the relative collision velocity will vary; hence so will e, and the relative importance of that assumption can be gauged. At a given temperature, a distribution of collision velocities and a corresponding distribution of coefficients of restitution occur. Varying T varies not only the average value of e, but also the amount of deviation around that average.

The variation in e gives rise to a velocity scale that is not present in the elastic case. All quantities given below are nondimensionalized with the particle diameter σ and the crossover velocity v_a at which the coefficient of restitution becomes a constant. In particular, the granular temperatures all scale with v_a^2.

Because inelastic collisions remove energy from the system, we must constantly add energy to achieve any sort of steady state. The situation is opposite that in simulations on nonequilibrium systems of elastic particles, where the constant energy input from the driving must be removed through an artificial means [37].

Stochastic heating is performed in one of three ways: (A) *White noise*—random kicks $\delta\mathbf{v}$ are added to particles' velocities, (B) *Random accelerations*—particles accelerate between collisions, and (C) *Boltzmann bath*—particle velocities are obliterated and replaced with velocities chosen from a Gaussian distribution. We discuss the motivation and implementation of each in turn.

A. White noise

Williams and MacKintosh [20] introduced white noise as a thermal bath for dissipative granular media. In their model, a random velocity is added to each particle's velocity during each time step Δt. The velocities added to each particle are not correlated with one another, nor are they correlated with the velocities added in the previous Δt. This model has the advantage that the equation of motion for particles between collisions may be written down as the Langevin equation

$$\frac{d^2 x_i}{dt^2} = \zeta_i, \qquad (19)$$

where x_i is the position of the ith particle and ζ_i is a Gaussian white noise term, i.e., $\langle \zeta_i(t)\zeta_j(t')\rangle = 2F\delta_{ij}\delta(t-t')$. The

fact that the heating can be analytically expressed makes its inclusion into kinetic theory possible.

This forcing is straightforward to include in our simulations. Rather than adding the random kicks to particles all at once, we kick $2r_k$ randomly chosen particles every time there is a collision. The number r_k, then, represents the ratio between the rate of kicks and the rate of collisions. If the kicks are totally random, the center of mass momentum of the system will fluctuate, but we desire that the heat bath can only change the fluctuational velocity, not the mean. To ensure that the mean velocity remains fixed, we apply random kicks to r_k particles:

$$\mathbf{v}_i \rightarrow \mathbf{v}_i + |\delta \mathbf{v}| \hat{\mathbf{r}}_i, \quad 1 \leq i \leq r_k. \tag{20}$$

The kicks themselves are all of the same size, $|\delta \mathbf{v}|$, but the directions $\hat{\mathbf{r}}_i$ are randomly chosen. Then, kicks in the opposite directions are applied to another r_k randomly chosen particles:

$$\mathbf{v}_i \rightarrow \mathbf{v}_i - |\delta \mathbf{v}| \hat{\mathbf{r}}_{i-r_k}, \quad r_k < i \leq 2r_k. \tag{21}$$

Because each kick requires recalculation of the kicked particle's collision list, we want to minimize the kick frequency. Empirically, we find that our results are independent of r_k for $r_k \geq 1$ and $r_k(\delta \mathbf{v})^2$ constant. This is not surprising, since the average length of r_k randomly oriented kicks of length $\delta \mathbf{v}$ is $\sqrt{r_k} \delta v$, and only the total kick between collisions matters when collisions occur. For this reason, we perform most of our simulations with $r_k = 1$, where the collision rate equals the kick rate.

B. Random accelerations: The air table model

While white noise forcing has the advantage that it can be incorporated into the kinetic theory relatively easily, it has the disadvantage that it does not model any particular real system. In most experiments, energy is added to the granular media through a boundary, causing gradients in the energy perpendicular to that boundary.

One experimental system is capable of producing homogeneous steady states, specifically, a collection of pucks on an air table [16,38]. Either due to inhomogeneities in the air flow or because the pucks are not perfectly parallel to the surface of the table, air flow accelerates the pucks uniformly from one collision to another [16], which counters the loss of energy due to inelastic collisions and produces a steady state.

In our model of the air table each particle moves under a uniform acceleration:

$$\mathbf{a}_i = a_0 \hat{\mathbf{r}}_i. \tag{22}$$

The magnitudes of all particle accelerations, a_0, are the same, but the directions, $\hat{\mathbf{r}}_i$, are randomly and uniformly chosen. When a collision occurs, $2r_k$ particles are given new $\hat{\mathbf{r}}_i$. In order to conserve total momentum, we hold the total acceleration of the particles at zero by giving exactly opposite accelerations to pairs of particles. Initially, each particle is paired with another, and these are given opposite accelerations. Later, when one particle is chosen and its acceleration
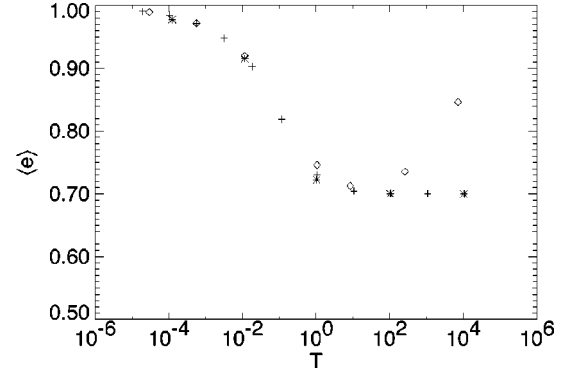

FIG. 1. Average coefficient of restitution vs T for $\nu = 0.5$, for the three forcing methods. $+$: White noise forcing, $\diamond$: Accelerated forcing, $*$: Boltzmann bath. As discussed in the text, T is nondimensionalized with v_a^2.

randomized, its partner particle is also given a new acceleration, opposite to the first particle's.

Experiments suggest that particles accelerate uniformly from collision to collision, with most of the changes in acceleration happening at collisions [16]. Therefore, $r_k = 1$ is probably a relatively good model for the air table experiments. As r_k increases, the particles feel a constant acceleration over a small temporal range. In the limit that $r_k \rightarrow \infty$, the model is the same as the white noise model, which is rate independent. In practice, we observe that the distribution of collision velocities for the accelerated particle model approaches that for the white noise model at $r_k \approx 8$.

Variation of coefficient of restitution with normal collision velocity is critical for simulations with the accelerated forcing, since inelastic collapselike collision sequences are more prevalent. A given pair of particles, accelerating towards one another, can hijack the collision sequence of the gas, rapidly recolliding with one another. If the coefficients of restitution are constant, this scenario will produce collapse. By allowing the collisions to become more elastic for decreasing relative velocities, however, collapse is prevented; eventually, the relative acceleration will change, and the particles will move apart. However, the large number of nearly elastic collisions produced by such a sequence causes the average coefficient of restitution to increase at the highest accelerations, as seen in Fig. 1.

C. The Boltzmann bath

Finally, we introduce a heat bath that approximates the assumption of molecular chaos. Molecular chaos assumes that the velocities of colliding particles are uncorrelated; particles collide, and before they collide with one another again, they collide with a large number of other particles, losing the memory of the initial condition. A strong heat bath can perform the same function if it replaces the particle velocities with new velocities chosen from a given distribution. If the heat bath interacts with the particles often enough, molecular chaos will be guaranteed. While this bath is wholly unphysical, it produces a situation in which the kinetic theory is expected to apply exactly; it is a useful check on calculations, and helps to elucidate the role of velocity correlations.

Implementation of the Boltzmann bath is simple. When two particles collide, $2r_k$ particles are randomly chosen and

given velocities chosen from a Boltzmann distribution with a specified temperature.

IV. HOMOGENEOUS FORCING, CORRELATIONS, AND THE EQUATION OF STATE

With any of the thermal baths just described, we can set up inhomogeneous states by varying the strength or rate of forcing over space. However, in the simplest case we force homogeneously. The simulations are performed for a variety of solid fractions, forcing rates, and forcing strengths for the three thermal baths.

The average coefficients of restitution for a number of runs at different temperatures are shown in Fig. 1. Note that at high temperatures, the average coefficient of restitution begins to rise for the accelerated forcing. This is due to the inelastic collapselike collision sequence described earlier for this forcing. As the magnitude of acceleration increases to produce higher temperatures, these multiple collisions become more and more important, leading to a large number of collisions with very low velocities, and so a high average coefficient of restitution.

In the state produced by homogeneous forcing, we can measure the single-particle distribution function, the temperature produced by the forcing, the pressure, the radial distribution function, velocity correlations, and loss rates. These quantities can be compared to the corresponding quantities for elastic simulations and to their assumed or calculated values from kinetic theory.

A. Single-particle velocity distributions

The lowest order approximation to f in the kinetic theories is usually chosen to be a Boltzmann distribution, the form of f for an undriven elastic gas. A driven inelastic gas, although it approaches a steady state, is by no means guaranteed to act like an undriven elastic gas. Nevertheless, the single-particle distribution functions measured from the simulation are all close to Boltzmann distributions, as seen in Fig. 2.

Overall, the accelerated forcing produces the strongest deviations from Maxwellian, and the Boltzmann bath, unsurprisingly, produces the least deviation. In all cases, the deviations become stronger as the density and temperature increase (recall that increasing temperature has the same effect as decreasing the average coefficient of restitution). These deviations tend to flatten the distribution, increasing the probability in the tails and slightly in the peak, and decreasing the probability in between, as displayed in Fig. 3. Similar types of deviations, but much stronger, have been observed in experiments on a dilute, vertically oscillated granular layer [14].

B. Equation of state and the radial distribution function

The equation of state, (13), relates the pressure, density, and temperature to the coefficient of restitution and $G(\nu)$. As stated in Sec. II, kinetic theories often use Eq. (13), with $G(\nu)$ given by $G_{CS}(\nu)$, from Eq. (5) to calculate pressure. This prescription may fail, then, either due to an incorrect equation of state, or an inappropriate use of the Carnahan and Starling relation.
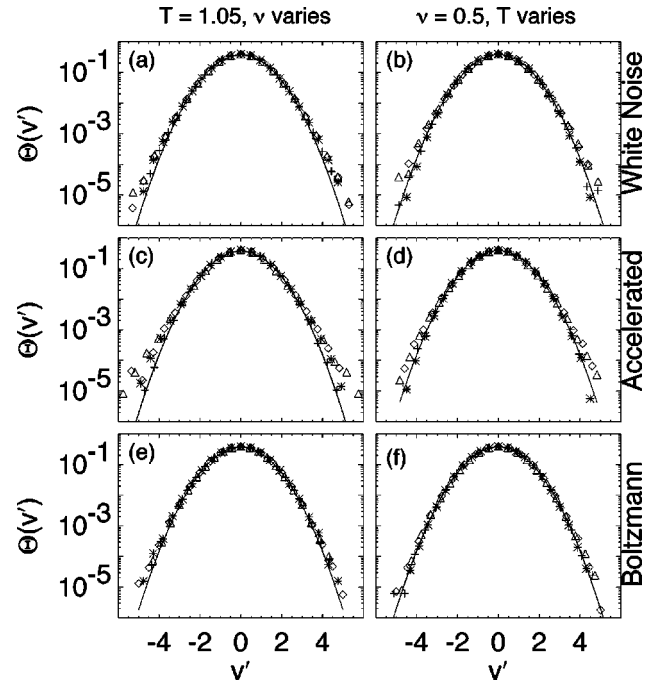

FIG. 2. Single-particle distribution function $\Theta(v')$ for (a) and (b) white noise forcing, (c) and (d) accelerated forcing, and (e) and (f) the Boltzmann bath, all with $r_k=1$. The velocities are scaled with the temperature T, so that $v'=v/\sqrt{T}$ and $\Theta(v')=\text{Pr}(v')\sqrt{T}$, where $\text{Pr}(v')$ is the probability distribution of v'. In the left column, the average temperature is approximately 1.05, and the solid fraction is varied ($+$: $\nu=0.1$, $*$: $\nu=0.4$, $\diamond$: $\nu=0.6$, $\triangle$: $\nu=0.8$.) In the right column, ν is fixed at 0.5 and the temperature is varied; (b) $T=1.93\times10^{-5}$ ($+$), 3.13×10^{-2} ($*$), 1.06 ($\diamond$), 1067 ($\triangle$). (d) $T=3.0\times10^{-5}$ ($+$), 1.1×10^{-2} ($*$), 1.05 ($\diamond$), 256 ($\triangle$). (f) $T=1.2\times10^{-5}$ ($+$), 1.1×10^{-2} ($*$), 1.02 ($\diamond$), 102 ($\triangle$). The solid curves are Boltzmann distributions.

No matter what the actual form of the equation of state, we can define a quantity

$$G_s(\nu)\equiv[(\pi\sigma^2 P/4\nu T)-1]/(1+e),$$

which explicitly satisfies Eq. (13). If the kinetic theory is correct, then
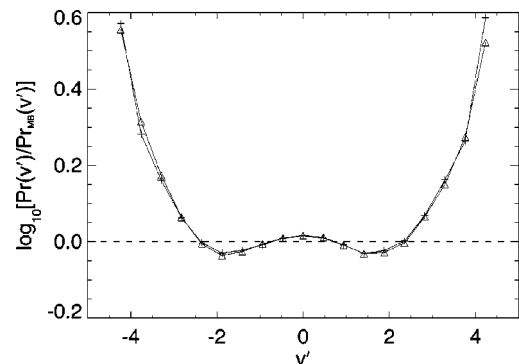
$$G_s(\nu)=\nu g(\sigma), \tag{23}$$

FIG. 3. The velocity distribution function Pr of $v'=v/\sqrt{T}$ from a simulation with accelerated forcing at $\nu=0.5$ and $T=1.05$, divided by Pr_{MB}, a Maxwell-Boltzmann distribution with $T=1.05$. The two curves are for the two velocity components.
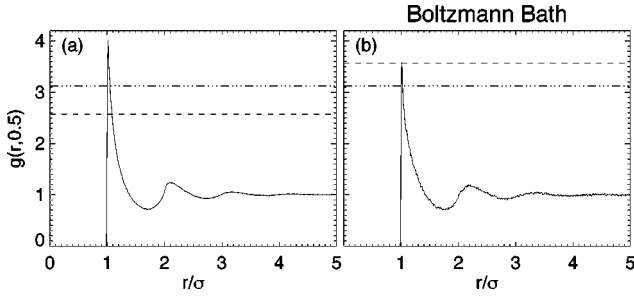
FIG. 4. $g(r)$ at $\nu=0.5, T=1.05$ for (a) white noise ($r_k=1$) and (b) Boltzmann ($r_k=4$) forcing. The dot-dashed lines represent the value of $g(\sigma)$ given by the Carnahan and Starling relation Eq. (5) for $\nu=0.5$, while the dashed lines show $G_s(\nu)/\nu$. For white noise forcing, $g(\sigma,\nu)$ coincides with neither line, while for the Boltzmann bath, $g(\sigma,\nu)$ coincides with $G_s(\nu)/\nu$.

as defined by Eq. (6). Testing the equation of state, then, is equivalent to testing Eq. (23).

Even if Eq. (23) is satisfied, the form of the radial distribution function at contact, $g(\sigma)$, may or may not be given by the Carnahan and Starling value of $G_{\mathrm{CS}}(\nu)/\nu$. Deviations from Eq. (13) and differences between the elastic and inelastic radial distribution functions can combine to produce $G_s(\nu)$ that is significantly different from $G_{\mathrm{CS}}(\nu)$, as given by Eq. (5). After discussing the method of calculating $G_s(\nu)$, we test each of the two effects given above, then show the resulting differences between $G_s(\nu)$ and $G_{\mathrm{CS}}(\nu)$.

The virial theorem of mechanics as applied to hard spheres can be used to calculate the equation of state [39,40],

$$PV = NT + \frac{\sigma}{2t_m} \sum_c \hat{\mathbf{k}} \cdot \Delta \mathbf{v}_i, \qquad (24)$$

where the sum is over all collisions that occur during the measurement time t_m, $\Delta \mathbf{v}_i$ is the change in the velocity of the ith particle due to the collision, and $\hat{\mathbf{k}}$ is the unit vector pointing from particle center to particle center. In this form, measurement of pressure reduces to measurement of the average particle energy and the average change in the normal velocity at collision.

Using Eq. (24) to measure pressure, and assuming the equation of state [Eq. (13)], we produce a measurement of $G(\nu)$, denoted $G_s(\nu)$, where the subscript s stands for simulation. This measured value of G will be used to test Eq. (23) and compared to the Carnahan and Starling value $G_{\mathrm{CS}}(\nu)$ from Eq. (5). Accurate characterization of $G(\nu)$ is important, because it occurs in the expressions for transport coefficients.

To investigate the radial distribution function and the equation of state, we plot $g(r,\nu)$ for a run with white noise forcing and a run forced with a Boltzmann bath in Fig. 4. Each plot also indicates the value of $g(\sigma,\nu)$ predicted by Eq. (23), as well as that predicted by Eq. (5), respectively testing the equation of state, and the Carnahan and Starling relation for the radial distribution function.

While $G_s(\nu)=\nu g(\sigma,\nu)$ for the Boltzmann forcing, this does not hold for the white noise forcing or the accelerated forcing (not shown). Recalling that the Boltzmann driving represents particles in contact with a highly randomizing bath, we conclude that this failure of the equation of state, (13), is due to incomplete randomization of particle velocities through collisions, or in short, a breakdown of molecular chaos.
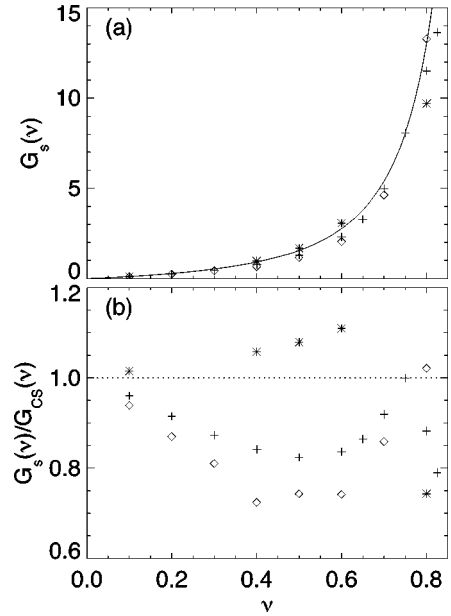

FIG. 5. (a) $G_s(\nu)$ for inelastic hard disks driven by +: white noise forcing, $\diamond$: accelerated, and *: Boltzmann forcing. The solid curve is the Carnahan and Starling relation $G_{\mathrm{CS}}(\nu)$, given by Eq. (5). (b) The ratio of $G_s(\nu)$ to $G_{\mathrm{CS}}(\nu)$. All runs have $r_k=1$ and $T=1.05$.

Furthermore, for neither forcing type does Eq. (5), the Carnahan and Starling relation for $G_{\mathrm{CS}}(\nu)$, properly predict $g(\sigma,\nu)$; rather, inelastic particles are more likely to be nearly in contact than elastic particles at the same density and temperature.

For inelastic particles with each type of forcing, $g(\sigma) > G_{\mathrm{CS}}(\nu)/\nu$. For either white noise or accelerated forcing, inelasticity also undermines the equation of state through the formation of velocity correlations, as shown in the following section. These two effects cancel each other to some degree; to assess the final result of using $G_{\mathrm{CS}}(\nu)$ and the equation of state, Eq. (13) in models, we calculate $G_s(\nu)$ for the three types of forcing as ν varies. The results are shown in Fig. 5. For ν below ≈ 0.675, where elastic particles undergo a phase transition to an ordered state [28], the white noise and accelerated runs produce lower G than elastic runs; Boltzmann runs have $G_s(\nu)$ slightly above the elastic values.

As the temperature decreases, $e \rightarrow 1$, and the values of $G_s(\nu)$ must approach the elastic values. Therefore, $G_s(\nu)$ must be temperature dependent; this dependence is shown in Fig. 6, along with the value of $G_s(\nu)$ given by Eq. (5). As T decreases, the inelastic $G_s(\nu)$ approaches the elastic G, and at high T, where e is independent of T, $G_s(\nu)$ becomes independent of T. As for the single-particle distributions, the accelerated forcing shows the greatest deviation from the elastic behavior.

C. Velocity correlations

Molecular chaos is the assumption that particle velocities are uncorrelated. Knowing the velocity of one of a pair of a colliding particle gives no information about the velocity of the other. In light of the behavior of G, and simulations that showed strong velocity correlations [21,17,12], we measure velocity-velocity correlation functions.
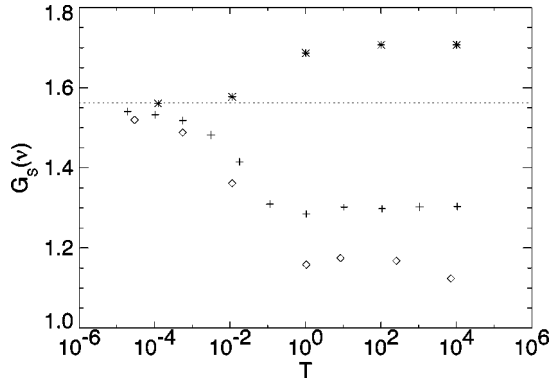
FIG. 6. $G_s(\nu)$ vs T for $\nu=0.5$. $+$: white noise, $\diamond$: accelerated, $*$: Boltzmann. The dotted line is the Carnahan and Starling relation $G_{CS}(\nu)$, given by Eq. (5), for $\nu=0.5$.

Given two particles, labeled 1 and 2, $\hat{\mathbf{k}}$ is a unit vector pointing from the center of 1 to the center of 2. Particle 1's velocity then has components $v_1^{\parallel}$ parallel to and $v_1^{\perp}$ perpendicular to $\hat{\mathbf{k}}$; likewise for particle 2. We define two correlation functions

$$\langle v_1^{\parallel} v_2^{\parallel}\rangle = \sum v_1^{\parallel} v_2^{\parallel}/N_r, \tag{25}$$

$$\langle v_1^{\perp} v_2^{\perp}\rangle = \sum v_1^{\perp} v_2^{\perp}/N_r, \tag{26}$$

where the sums are over N_r particles such that the distance between the two particles is within δr of r. If particle velocities are uncorrelated, $\langle v_1^{\parallel} v_2^{\parallel}\rangle$ and $\langle v_1^{\perp} v_1^{\perp}\rangle$ will both give zero.

The parallel and perpendicular velocity correlations are plotted in Fig. 7 for the three types of forcing and for elastic particles. Both for particles driven with white noise and accelerations, strong long-range velocity correlations are apparent, with more correlations produced by the accelerated forcing, consistent with its stronger deviations in the single-particle velocity distribution and in G. These correlations are not small, reaching as much as 40% of the temperature; typically, the perpendicular correlations are about one-half of the parallel correlations. Further, these correlations are long range—they extend the full length of the system. The parallel correlations drop to zero at $L/2$, while the perpendicular correlations reach zero around $r=10\sigma$, and have a negative value but zero derivative at $L/2$. The long-range nature of the correlation is not due to the size of the computational cell. Similar cell-filling correlations were observed in runs 4, 16, and 64 times larger [41].

For the Boltzmann forcing, some correlations are visible at very short range; inelastic collisions generate short-range velocity correlations, which are destroyed by the heat bath before they can propagate to larger length scales.

D. Loss rate

The loss rate of temperature due to inelastic collisions, γ, divided by the rate calculated from kinetic theory, γ_0 [see Eq. (14)], is shown for the three forcing methods as a functions of T in Fig. 8(a) and ν in Fig. 9(a). For the calculation
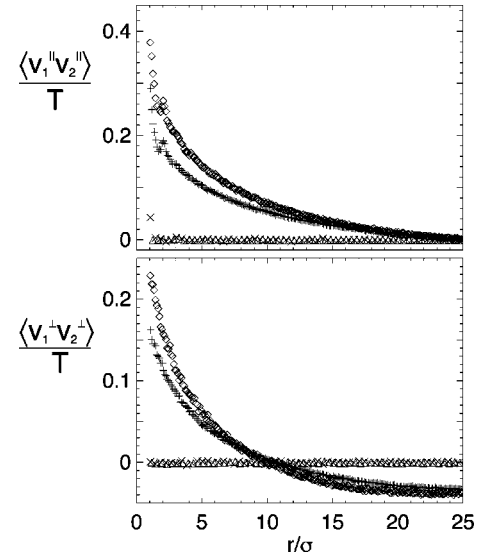

FIG. 7. Velocity correlations as a function of particle separation at $\nu=0.5, T=1.05$ for white noise $(+)$, accelerated $(\diamond)$, Boltzmann forcing $(\times)$, and elastic particles $(\triangle)$. Each curve is built from around 100 frames separated in time by 100 collisions per particle, and $\delta r = \sigma/10$. Both the elastic particles and the particles forced with the Boltzmann bath have essentially zero correlation over most of the range. The Boltzmann bath shows positive correlations only at very short range.

of γ_0, G was taken from the equation of state measurements, and the average e within a run was used. Most surprising is the increased loss rate over kinetic theory at relatively low temperature.

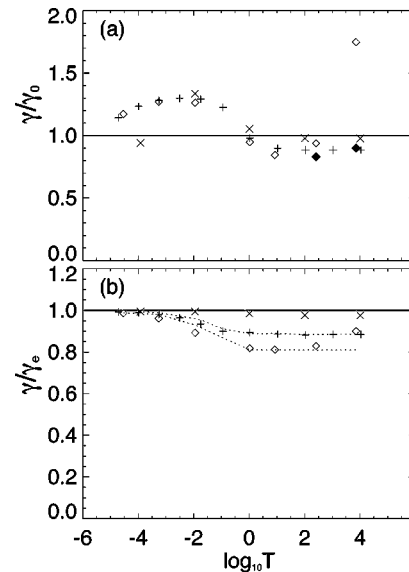The calculation of γ requires only the evaluation of

FIG. 8. Temperature dependence of loss rate with $\nu=0.5$. (a) γ/γ_0, where the kinetic theory result γ_0 [Eq. (14)] assumes a velocity-independent restitution coefficient. (b) γ/γ_e, where γ_e takes into account the velocity dependence of e. The symbols denote the type of forcing: $+$, white noise; $\diamond$, accelerated; $\times$, Boltzmann. The dotted lines show $(\sqrt{\pi}/4\sqrt{T})\langle v_n^2\rangle_c/\langle v_n\rangle_c$ for the white noise and accelerated runs; see Eq. (33).

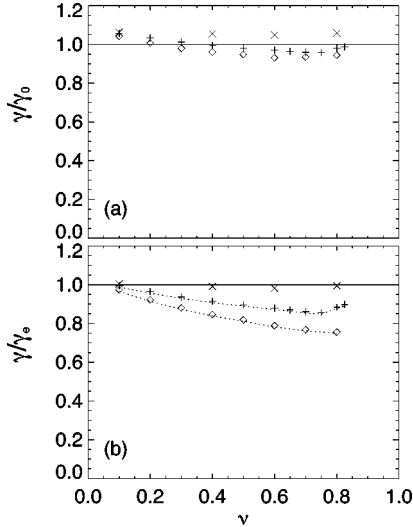FIG. 9. (a) γ/γ_0 and (b) γ/γ_e versus ν at $T=1.05$. The symbols denote the type of forcing: $+$, white noise; $\diamond$, accelerated; $\times$, Boltzmann.

$$\gamma=\frac{\sigma}{2}\int\int\frac{1}{4}(1-e^2)(\mathbf{v}_{12}\cdot\hat{\mathbf{k}})^3 f^{(2)}(\mathbf{v}_1,\mathbf{v}_2)d\Omega d\mathbf{v}_1 d\mathbf{v}_2, \tag{27}$$

where $d\Omega$ is the angle element. This expression simply averages the energy lost per collision,

$$\frac{1}{4}(1-e^2)v_n^2=\frac{1}{4}(1-e^2)(\mathbf{v}_{12}\cdot\hat{\mathbf{k}})^2 \tag{28}$$

over all possible collisions. The remaining factor of $(\mathbf{v}_{12}\cdot\hat{\mathbf{k}})$ takes into account the fact that grains traveling towards one another more rapidly are more likely to collide during any given time interval.

The kinetic theory result for the loss rate, Eq. (14), follows from the collisional integral, Eq. (27), under two assumptions: molecular chaos, which ought to be a more reasonable assumption at lower temperatures, and the independence of e on the variables of integration, so that it is pulled out of the integral as a constant. At lower temperature, where the variation of e with v_n leads to a distribution of e at a given temperature, the second assumption fails. As temperature drops still farther, the spread of e reduces, since e is bounded from above by 1; at the very lowest T, γ does approach γ_0.

Substituting the function form of $e(v_n)$, Eq. (18), into the collisional integral, Eq. (27), assuming molecular chaos, and performing the integrations, we arrive at an equation for $\gamma = \gamma_e$ that takes into account the variation of e with v_n:

$$\gamma_e=\frac{4\nu G\sqrt{T}}{\sigma^3\pi^{3/2}}[(1-e_0^2)(v_a^2+4T)\exp(-v_a^2/4T)+4I], \tag{29}$$

where

$$I=2^{1+\beta}AT^{1+\beta/2}[\Gamma(2+\tfrac{1}{2}\beta)-\Gamma(2+\tfrac{1}{2}\beta,v_a^2/4T)]$$
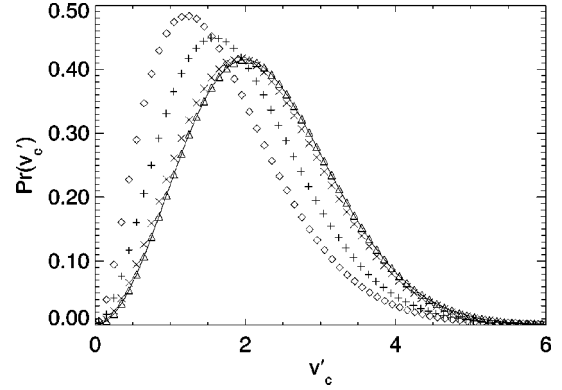$$-A^2 2^{2\beta}T^{1+\beta}[\Gamma(2+\beta)-\Gamma(2+\beta,v_a^2/4T)], \tag{30}$$

FIG. 10. Probability distribution of $v_c'\equiv|\mathbf{v}_1-\mathbf{v}_2|/\sqrt{T}$, the magnitude of relative velocities at collision for different forcings, white noise ($+$), accelerated ($\diamond$), Boltzmann ($\times$), and for elastic particles ($\triangle$), all at $\nu=0.5$ and $T=1.05$. The solid curve is the distribution predicted by uncorrelated collisions between particles chosen from Boltzmann distributions, $(1/2\sqrt{\pi T^3})v_c^2 e^{-v_c^2/4T}$. Positive velocity correlation of nearby particles causes a reduction in the collision velocities, and hence a reduction in γ.

$\Gamma(a)$ is the gamma function, and $\Gamma(a,b)$ is the incomplete gamma function. In the limit that $v_a\rightarrow 0$, $\gamma_e\rightarrow\gamma_0$.

Figures 8(b) and 9(b) show γ/γ_e for the same simulations shown in Figs. 8(a) and 9(a). Taking the variations in e into account removes the underestimation of γ. In the revised picture, γ approaches γ_e at low T and at low ν, but as either increases, γ drops from the value predicted by γ_e. This is due to the velocity correlations produced by the inelasticity. Locally, particles are moving together, reducing collision velocities and collision frequencies, thereby reducing the loss rate; see Fig. 10. For the Boltzmann forcing, velocity correlations are wiped out, and γ is close to γ_e.

Writing γ in terms of average quantities makes its dependence on the collision velocity more explicit. The loss rate is identically equal to the average energy lost per collision, $\langle\Delta E\rangle_c$, times the average collision frequency per volume f/V,

$$\gamma=\langle\Delta E\rangle_c f/V=\frac{1}{4}(1-e^2)\langle v_n^2\rangle_c f/V, \tag{31}$$

where the c subscript denotes an average over collisions, and assuming again that e is independent of collision velocity. Similarly, the virial equation of state, Eq. (24), in terms of average quantities is

$$P=(4/\pi\sigma^2)\nu T\left(1+\frac{V\sigma}{d}f\frac{1+e}{2}\langle v_n\rangle_c\right). \tag{32}$$

Solving for f in terms of G from Eqs. (13) and (32), and substituting this into Eq. (31) we obtain

$$\gamma=\frac{(1-e^2)G}{\sigma}\frac{\langle v_n^2\rangle_c}{\langle v_n\rangle_c}nT. \tag{33}$$

If the distribution of relative normal velocity at collision is equal to that predicted by molecular chaos, $P(v_n)=(1/2T)v_n\exp(-v_n^2/4T)$, then $\langle v_n^2\rangle_c=4T$ and $\langle v_n\rangle_c=\sqrt{\pi T}$, so that $\gamma=\gamma_0$ is recovered.
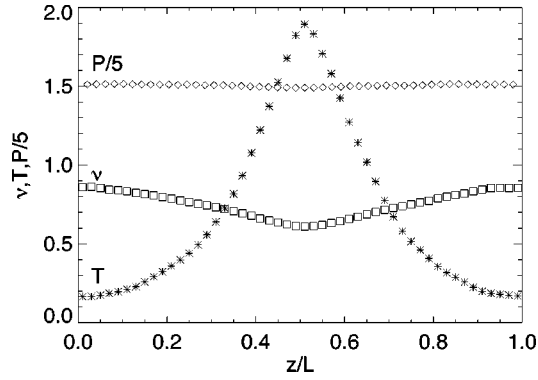
FIG. 11. Profiles of $*$: T, $\square$: ν, and $\diamond$: $P/5$ for inhomogeneous forcing in which the magnitude of the acceleration depends linearly on the distance from $z/L=\frac{1}{2}$. The pressure is nearly constant, so that the variation in T induces a variation in ν through the equation of state. For this run, the average solid fraction is 0.75.

As seen in Fig. 10, however, the distribution of collision velocities is different from the molecular chaos values due to the presence of velocity correlations. To show that this deviation accounts for the remaining difference between γ and γ_e, $\langle v_n^2 \rangle_c$ and $\langle v_n \rangle_c$ were calculated in the simulations. Their ratio, normalized by the molecular chaos value $4\sqrt{T/\pi}$ is plotted in Figs. 8(b) and 9(b) as dotted lines. The change in the relative collision velocity tracks the change in γ, except for high temperature accelerated runs, in which repeated two-particle collisions become important.

V. INHOMOGENEOUS FORCING AND TRANSPORT COEFFICIENTS

So far, we have been concerned with homogeneous forcing. By using applied forcing that varies spatially, we can induce inhomogeneous steady states. Then, by measuring fluxes, transport coefficients are calculated, and compared to kinetic theory. Inhomogeneous states have only been calculated for the accelerated forcings; measurements for the homogeneous state show that deviations from the elastic case are strongest in this case.

A. Thermal conductivity

Recall that with the accelerated forcing, the direction of the accelerations of particles fluctuated at a fixed rate, but the magnitude was always the same. To induce a thermal gradient in the simulation, we allow the magnitude of the acceleration to vary in space. Specifically, when the acceleration of a particle is to be rotated, the magnitude of its acceleration is given by

$$a_0[1-|(z-\tfrac{1}{2}L)/(\tfrac{1}{2}L)|], \quad (34)$$

i.e., we apply a linear gradient in the forcing, dependent on one spatial direction (z), peaked in the center of the cell and falling to zero at the periodic boundary. In order to preserve the center of mass momentum, the partner particle receives the opposite acceleration, regardless of its position in the cell, as described in Sec. III B.

Under this forcing, a stable thermal profile develops, as seen in Fig. 11. The system reaches a mechanical equilib-
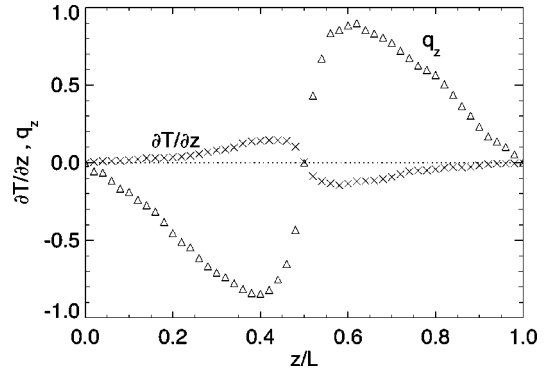
rium; the pressure is nearly constant in z. Constant P and varying T imply varying ν through the equation of state, and this variation is observed.

The cell is divided into 50 slabs along z for measurement purposes; for each slab, snapshots allow calculation of the average T and ν within. Because the pressure may in principle vary over space, its measurement using the virial fails. Pressure is measured at the interfaces between the slabs by keeping track of the normal (z) momentum flux through these boundaries, both due to particles freely traveling through them, and due to collisions between particles that lie in different slabs. As in Sec. IV D, G is calculated from Eq. (13) using the measured pressure. In addition, the energy added due to the forcing and the energy lost due to inelastic collisions are separately accounted for for each slab. The difference between the energy gain and loss in a given slab must, in a steady state, be made up for by the difference in energy flux through its two boundaries, so that the net rate of change of the energy in the slab is zero. Assuming that the energy flux through the line at $z=(0,L)$ is zero due to symmetry allows calculation of $\mathbf{q}_z$, the heat flux through each slab boundary; see Fig. 12.

Once $\mathbf{q}_z$ and $\partial T/\partial z$ are calculated, Fourier's heat law, Eq. (12), can be used to calculate the thermal conductivity κ. The results of many simulations, holding the average ν at 0.75, but varying a_0 in Eq. (34) and therefore the size of the thermal gradient, are shown in Fig. 13, and are compared to the result of Enskog theory, as given by Eq. (17). At low temperatures, Enskog theory does a good job predicting κ.
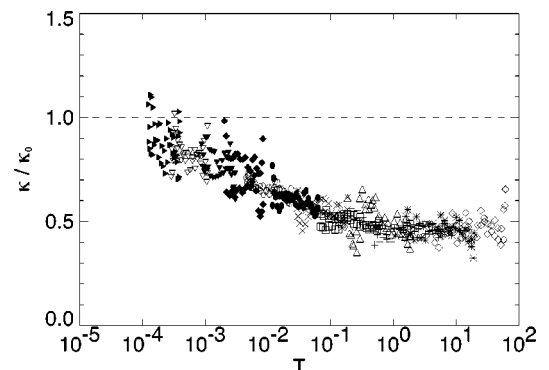

FIG. 12. The thermal gradient ($\times$) and heat flux ($\triangle$) for the run shown in Fig. 11.

FIG. 13. Ratio of κ measured from simulations to κ_0 from Enskog theory [Eq. (17)]. Each symbol denotes a different run, but for each run, the average solid fraction is 0.75.
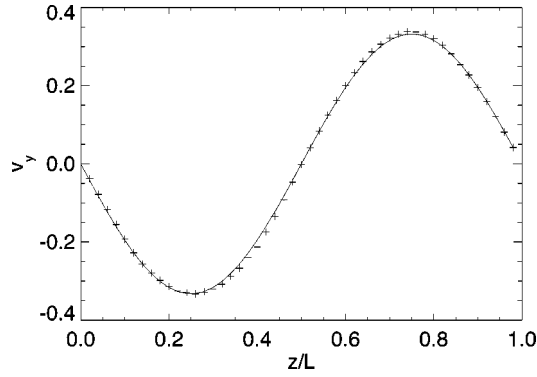
FIG. 14. Average velocity in the y direction as a function of z at $T=0.21$, $\nu=0.6$. The solid line is sinusoidal.

FIG. 15. Normal stress difference divided by pressure as a function of $1-e$. The line has slope 1.

However, as the temperature increases and $e(v_n)$ decreases, Enskog theory does worse; at the highest temperatures, Enskog theory overestimates the thermal conductivity by a factor of 2.

Note that this calculation does not test Fourier's law; rather we assume that Fourier's law is correct, and use it to calculate κ. Analysis based on closures of the Boltzmann equation predicts a term in the heat flux proportional to the density gradient [42]. If such a term had a sizable magnitude and were ignored, it would cause a reduction in the observed κ.

B. Shear viscosity

Spatial inhomogeneity in the magnitude of the forcing led to a stationary inhomogeneous temperature field, allowing measurement of heat flux and thermal conductivity; spatial inhomogeneity in the mean of one forcing component leads to a stationary inhomogeneous velocity field, allowing measurement of the momentum flux and the shear viscosity. In particular, particle accelerations are chosen according to

$$a_y = a_0[0.01 \sin(2\pi z/L) + \psi_0], \qquad (35)$$

$$a_z = a_0 \psi_1, \qquad (36)$$

where ψ_0 and ψ_1 are numbers chosen randomly from a Gaussian distribution with zero mean and standard deviation of 1.

This forcing produces steady states with velocity, temperature, density, and stress fields like that shown in Fig. 14. The velocity profile is nearly sinusoidal in z, and the temperature, pressure, and solid fraction are essentially independent of z. In the simulations discussed so far, we have only considered the scalar quantity $T = \langle (v - \langle v \rangle)^2 \rangle / D$, where D is the number of dimensions and the $\langle \rangle$ denote averages over particles. This temperature is more generally the trace of the temperature tensor:

$$T_{ij} = \langle (v_i - \langle v_i \rangle)(v_j - \langle v_j \rangle) \rangle, \qquad (37)$$

where i,j range over the directions, and v_i denotes the ith component of the velocity. In principle, T_{yy} need not equal T_{zz} if the rate at which fluctuational energy is traded between the directions is slower than the rate at which it is added anisotropically; such is the case in a vertically oscillated granular layer, where vertical fluctuational energy can be
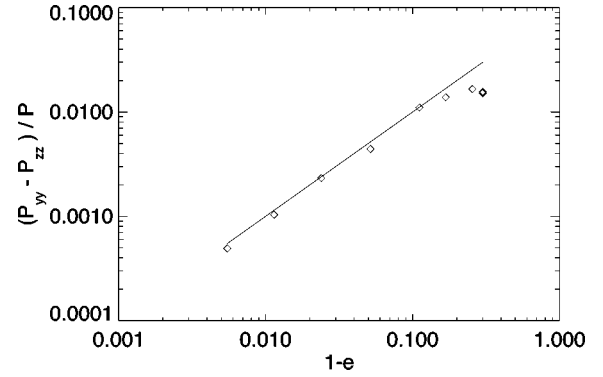
twice that of the horizontal. Introducing a bias in the acceleration of only 1%, however, does not introduce anisotropy into T; for larger shear rates this is not the case. To study the simplest case, we restrict our simulations to biases of 1%.

Due to their dissipative nature, many granular flows are supersonic. In supersonic shear flow, the nearly parallel particle paths lead to extremely long mean free paths, casting doubt on a continuum approach [8]. A small bias in the acceleration allows the shear flows to remain subsonic, so that mean free paths remain smaller than the system size.

In Sec. V A we described calculation of the pressure by measuring the normal momentum flux through planes. Measuring the tangential flux through the planes, and introducing a second set of planes orthogonal to the first, allows calculation of the full four-component pressure tensor. As seen in Fig. 15, the pressure tensor is anisotropic even though T is isotropic; the anisotropy increases as T increases, or e decreases. For $e \approx 1$, the stress difference is approximately proportional to $1-e$, but the variation in e within a given run probably plays a role, as it did in the loss rate; see Fig. 15. For these runs, G is calculated from Eq. (13) using the trace of the measured pressure tensor.

For each run at fixed T, we can test Newton's viscosity law,

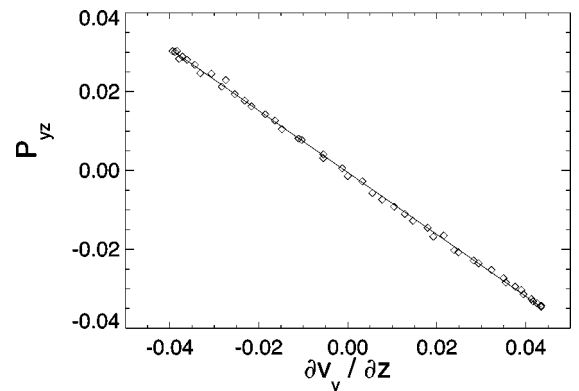$$P_{yz} = -\mu \frac{\partial v_y}{\partial z}, \qquad (38)$$

FIG. 16. The yz component of the pressure tensor versus the corresponding velocity derivative for the run of Fig. 14. The slope of the best fit line is $-\mu$.
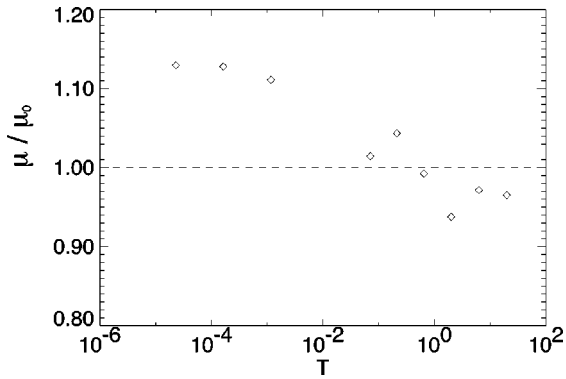
FIG. 17. Viscosity, normalized by the Enskog value μ_0, as a function of T, for $\nu = 0.6$.

where the viscosity μ is a constant of proportionality. A typical result is shown in Fig. 16, where the linear relation of Eq. (38) is shown to hold. The slopes of these curves then provide values for μ which can be compared to the Enskog result from Eq. (16); the results are shown in Fig. 17.

Unlike the loss rate and thermal conductivity, we find that the Enskog theory underestimates the shear viscosity at lower temperatures. However, the trend of decreasing transport with increasing T is the same. Even for elastic particles, Enskog theory is not expected to work to arbitrarily high solid fractions; as density increases, deviations from Enskog theory are expected. As the inelasticity of particles increases, velocity correlations increase, reducing collisional momentum transport and lowering the viscosity.

VI. CONCLUSION

Volumetric driving of granular media leads to nearly stationary states that are amenable to comparison with kinetic theory, allowing us to test the six points of kinetic theory listed in Sec. I. Volumetric driving is atypical; most granular systems are forced through a boundary. However, the stationary states achieved here are the simplest testing ground for kinetic theory, and provide an upper bound on the applicability of kinetic theories in the style of Jenkins and Richman [5–7,25,26] to real systems.

Given that many of our simulations involve coefficients of restitution that are not near 1, the general level of agreement with kinetic theory is surprisingly good, suggesting that continuum approaches to dissipative granular media are capable not only of qualitative, but also quantitative descriptions of real systems. We now discuss each of the six points in turn.

Single-particle distribution functions are nearly Boltzmann. For all forcing types, temperatures (coefficients of restitution), and densities, the single-particle distribution functions are close to Boltzmann distributions (Fig. 2). The deviations from Gaussian (Fig. 3) are consistent with but much smaller than those seen in experiments on thin (<1 layer deep) oscillated granular media [14]. In those experiments, deviations appear to be due to spontaneous spatial variations in temperature that are not taken into account in the analysis [43]; such variations become large for cooling, unforced granular media. The smaller deviations exhibited in our simulations may represent smaller temperature fluctuations.

Particle velocities are correlated. Standard kinetic theory assumes molecular chaos: particle velocities are uncorrelated. In our simulations, as in simulations of cooling granular media [17], strong velocity correlations (Fig. 7) with a characteristic vortex structure [41] develop. In the steady state, these correlations extend over the entire cell. Molecular chaos is not required for kinetic theory, but a closure for the kinetic equation is critical. Similar considerations have led van Noije *et al.* [13] to apply ring kinetic theory [44], which allows for correlations in particle velocities, to a granular system.

Spatial correlations are stronger than predicted by the Carnahan and Starling relation [Eq. (5)]. Even for simulations using the Boltzmann bath, in which velocity correlations are removed, the effect of inelasticity is to increase the amount of spatial correlation at $r = \sigma$ [Fig. 4(b)]. In other words, particles are more likely in the inelastic case to be close to one another than elastic particles in the same thermodynamic state. The size of this effect is dependent on the inelasticity, but can be greater than 15%.

The equation of state overestimates the collisional contribution to pressure because it ignores velocity correlations. The factor in the equation of state describing the contribution from collisions, $G_s(\nu)$, as calculated from the measurement of pressure and the equation of state, is smaller for white noise and acceleration forcings than that predicted by the Carnahan and Starling relation [Eqs. (5) and (6)], denoted $G_{CS}(\nu)$ (Fig. 5). In turn, $G_{CS}(\nu)$ is smaller than the actual $G(\nu) \equiv \nu g(\nu)$, as discussed in the previous paragraph. Because velocity correlations were ignored in the derivation of the equation of state (13), the pressure due to collisions that G describes is overestimated. To some degree, the increased positional correlation and increased velocity correlation work against one another; the first increases the collision frequency, while the latter decreases it. The net result is that the $G_s(\nu)$ from the pressure measurement is closer to Carnahan and Starling, Eq. (5), $G_{CS}(\nu)$ than if there were only velocity correlations [Fig. 4(a)].

Newton's stress law works well for low stress. Even at the highest inelasticity, $e = 0.7$, no deviations from a linear relation between stress and strain rate [Eq. (11)] were observed (Fig. 16). However, in order to keep the temperature isotropic, we have limited ourselves to cases in which $v^2 < T$; many flows of interest are supersonic, with average velocities much larger than $\sqrt{T}$. Because κ depends on T, and therefore on position, Fourier's heat law was not tested in the same manner that Newton's viscosity law was.

Temperature loss rate γ and thermal conductivity κ are reduced by inelasticity, while shear viscosity μ is predicted relatively well by Enskog theory. For increasing inelasticity or density in homogeneously forced runs, velocity correlations also increase. As a consequence, the relative collision velocity decreases (Fig. 10), leading to a reduction in the temperature loss rate due to inelastic collisions [Figs. 8(b) and 9(b)]. In the most severe cases examined, once corrected for variations in e, this deviation could be as high as 20%. Inhomogeneously forced runs allowed calculation of μ, and, assuming Fourier's law, κ; μ never deviated from the prediction of Enskog theory by more than 15% (Fig. 17), while κ was found to be smaller than predicted by a factor of 2 for high inelasticities (Fig. 13). This differential success sug-

gests that velocity correlations, which should be present in both cases, are not responsible for the large reduction in κ. Rather, the inelasticity itself may be the cause. Enskog theory, applied to granular media, assumes that $e \approx 1$; the values of κ_0 and μ_0 are the same as those for elastic particles. When grains collide, energy is dissipated, so that the amount transported collisionally is necessarily reduced as e decreases. On the other hand, momentum is still conserved, so that μ is relatively unaffected. Also, some deviation from Enskog theory is possible due to a term in the heat flux proportional to density gradients.

The results described above suggest a number of avenues for future research. First, measurements of viscosity should be extended into the supersonic regime. Second, more extensive calculations of thermal conductivity at different densities, and with different spatial forcings, should be undertaken to ascertain the role of density gradients. Third, time-dependent calculations should be performed, allowing measurement of the bulk viscosity. Such calculations should also provide measurements of the frequency dependence of the transport coefficients, which may be relevant for oscillated granular media. Fourth, the granular continuum equations can be used to perform stability calculations on problems such as vertically oscillated granular media [45,46]. Finally, new forcing geometries should be explored, allowing direct comparison between particle simulations, continuum theories, and experiments.

[1] C. S. Campbell, Annu. Rev. Fluid Mech. **2**, 57 (1990).

[2] H. M. Jaeger, S. R. Nagel, and R. P. Behringer, Phys. Today **49** (4), 32 (1996).

[3] F. Melo, P. Umbanhowar, and H. L. Swinney, Phys. Rev. Lett. **72**, 172 (1994).

[4] J. R. de Bruyn, C. Bizon, M. D. Shattuck, D. Goldman, J. B. Swift, and H. L. Swinney, Phys. Rev. Lett. **81**, 1421 (1998).

[5] C. K. K. Lun, S. B. Savage, D. J. Jeffrey, and N. Chepurniy, J. Fluid Mech. **140**, 223 (1983).

[6] J. T. Jenkins and M. W. Richman, Arch. Ration. Mech. Anal. **87**, 355 (1985).

[7] J. T. Jenkins and M. W. Richman, Phys. Fluids **28**, 3485 (1985).

[8] M.-L. Tan and I. Goldhirsch, Phys. Rev. Lett. **81**, 3022 (1998).

[9] L. P. Kadanoff, Rev. Mod. Phys. **71**, 435 (1999).

[10] C. Bizon, M. D. Shattuck, J. B. Swift, W. D. McCormick, and H. L. Swinney, Phys. Rev. Lett. **80**, 57 (1998).

[11] C. Bizon, M. D. Shattuck, J. R. de Bruyn, J. B. Swift, W. D. McCormick, and H. L. Swinney, J. Stat. Phys. **93**, 449 (1998); color pictures of granular convection can be found at http://chaos.ph.utexas.edu/errata/bizon98a.html.

[12] T. P. C. van Noije, M. H. Ernst, E. Trizac, and I. Pagonabarraga, Phys. Rev. E **59**, 4326 (1999).

[13] T. P. C. van Noije, M. H. Ernst, and R. Brito, Physica A **251**, 266 (1998).

[14] J. S. Olafsen and J. S. Urbach, Phys. Rev. Lett. **81**, 4369 (1998).

[15] W. Losert, D. G. W. Cooper, J. Delour, A. Kudrolli, and J. P. Gollub, e-print cond-mat/9901203.

[16] L. Oger, C. Annic, D. Bideau, R. Dai, and S. B. Savage, J. Stat. Phys. **82**, 1047 (1996).

[17] J. A. G. Orza, R. Brito, T. P. C. van Noije, and M. H. Ernst, Int. J. Mod. Phys. C **8**, 953 (1998).

[18] T. P. C. van Noije, M. H. Ernst, and R. Brito, Phys. Rev. E **57**, R4891 (1998).

[19] E. L. Grossman, T. Zhou, and E. Ben-Naim, Phys. Rev. E **55**, 4200 (1997).

[20] D. R. M. Williams and F. C. MacKintosh, Phys. Rev. E **54**, R9 (1996).

[21] M. R. Swift, M. Boamfă, S. J. Cornell, and A. Maritan, Phys. Rev. Lett. **80**, 4410 (1998).

[22] A. Puglisi, V. Loreto, U. M. B. Marconi, A. Petri, and A. Vulpini, Phys. Rev. Lett. **81**, 3848 (1998).

[23] S. Chapman and T. G. Cowling, *The Mathematical Theory of Non-uniform Gases* (Cambridge University Press, London, 1970).

[24] C. K. K. Lun, J. Appl. Mech. **54**, 47 (1987).

[25] C. K. K. Lun, J. Fluid Mech. **233**, 539 (1991).

[26] A. Goldshtein and M. Shapiro, J. Fluid Mech. **282**, 75 (1995).

[27] N. F. Carnahan and K. E. Starling, J. Chem. Phys. **51**, 635 (1969).

[28] B. J. Alder and T. E. Wainwright, Phys. Rev. **127**, 359 (1962).

[29] D. M. Gass, J. Chem. Phys. **54**, 1898 (1970).

[30] B. D. Lubachevsky, J. Comput. Phys. **94**, 255 (1991).

[31] M. Marín, D. Risso, and P. Cordero, J. Comput. Phys. **109**, 306 (1993).

[32] S. McNamara and W. R. Young, Phys. Fluids A **4**, 496 (1992).

[33] S. McNamara and W. R. Young, Phys. Rev. E **50**, R28 (1994).

[34] W. Goldsmith, *Impact* (Edward Arnold Ltd., London, 1960).

[35] C. V. Raman, Phys. Rev. **12**, 442 (1918).

[36] D. Goldman, M. D. Shattuck, C. Bizon, W. D. McCormick, J. B. Swift, and H. L. Swinney, Phys. Rev. E **57**, 4831 (1998).

[37] D. J. Evans and G. P. Morriss, *Statistical Mechanics of Non-equilibrium Liquids* (Academic Press, San Diego, 1990).

[38] I. Ippolito, C. Annic, J. Lemaître, L. Oger, and D. Bideau, Phys. Rev. E **52**, 2072 (1995).

[39] J. O. Hirschfelder, C. F. Curtiss, and R. B. Byrd, *Molecular Theory of Gases and Liquids* (Wiley, New York, 1954).

[40] D. C. Rapaport, *The Art of Molecular Dynamics Simulation* (Cambridge University Press, Cambridge, England, 1980).

[41] C. Bizon, M. D. Shattuck, J. B. Swift, and H. L. Swinney, in *Dynamics: Models and Kinetic Methods for Nonequilibrium Many-Body Systems*, NATO ASI Series E: Applied Sciences, edited by J. Karkheck (Kluwer Academic Publishers, Dordrecht, in press).

[42] J. J. Brey, J. W. Duffy, and A. Santos, J. Stat. Phys. **87**, 1051 (1997).

[43] J. S. Urbach (private communication).

[44] M. H. Ernst, E. H. Hauge, and J. M. J. van Leeuwen, Phys. Rev. A **4**, 2055 (1971).

[45] C. Bizon, Ph.D. thesis, University of Texas at Austin, 1998.

[46] C. Bizon, M. D. Shattuck, and J. B. Swift (unpublished).